

Coherence properties of Kerr frequency combs

Miro Erkintalo* and Stéphane Coen

Physics Department, The University of Auckland, Private Bag 92019, Auckland 1142, New Zealand

*Corresponding author: m.erkintalo@auckland.ac.nz

Compiled September 17, 2018

We use numerical simulations based on an extended Lugiato-Lefever equation (LLE) to investigate the stability properties of Kerr frequency combs generated in microresonators. In particular, we show that an ensemble average calculated over sequences of output fields separated by a fixed number of resonator roundtrips allows the coherence of Kerr combs to be quantified in terms of the complex-degree of first-order coherence. We identify different regimes of comb coherence, linked to the solutions of the LLE. Our approach provides a practical and unambiguous way of assessing the stability of Kerr combs that is directly connected to an accessible experimental quantity. © 2018 Optical Society of America

OCIS codes: 230.5750, 190.5530, 190.4380, 030.1640

Kerr microresonators offer a promising route towards miniaturization of the frequency comb technology, which has led to intense investigations of “Kerr combs” over the last few years [1–10]. Despite being excited by continuous-wave (cw) light, these combs are still in some conditions underlined by ultrafast pulses in the form of localized dissipative structures known as temporal cavity solitons (CSs) [11–13]. This was initially suggested in [12] and subsequently demonstrated both theoretically [14–18] and experimentally [19]. The microresonator technology therefore also holds potential for on-chip generation of high repetition-rate pulse trains.

Stability is a key factor for many applications of frequency combs. Quantifying the noise properties of microresonator-based combs has, however, proven difficult. Radio-frequency measurements are hindered by large resonator free-spectral ranges (FSRs) [7, 8]. Additional optical heterodyning relaxes this limitation but is rather complex to implement [8, 19]. These two methods do not however easily reveal how noise varies across the comb and offer limited insights on time-domain properties. Comb coherence has also been inferred from autocorrelation-type temporal signals [6, 7], yet these are average measurements that are prone to misinterpretations [20]. An alternative method has been used in the context of supercontinuum (SC) frequency combs. Two independently generated SC were superimposed on a spectrometer, with the resulting spectral interference pattern providing direct evidence of the SC coherence [21]. Of course, the visibility of the interference fringes is simply the modulus of the wavelength-dependent complex degree of first-order coherence, which has been exploited to elucidate the mechanisms of SC coherence degradation both numerically [22, 23] and experimentally [24, 25]. In this Letter, we theoretically examine Kerr comb stability in light of this definition. Specifically, an ensemble average computed over spectral snapshots of the simulated intracavity field separated by a fixed number of resonator roundtrips allows the wavelength-dependent degree of coherence to be calculated. We report that the different comb dynamical regimes, previously identified in [16], exhibit qualitatively different coherence characteristics.

In our work, Kerr comb dynamics is modeled with a gener-

alized mean-field Lugiato-Lefever equation (LLE) [15–18],

$$t_R \frac{\partial E(t, \tau)}{\partial t} = \left[-\alpha - i\delta_0 + iL \sum_{k \geq 2} \frac{\beta_k}{k!} \left(i \frac{\partial}{\partial \tau} \right)^k + i\gamma L |E|^2 \right] E + \sqrt{\theta} E_{\text{in}}. \quad (1)$$

Here t is the slow time describing the evolution of the intracavity electric field envelope $E(t, \tau)$ over subsequent resonator roundtrips while τ is a fast time defined in a reference frame traveling at the group velocity of the driving field with cw amplitude E_{in} . $t_R = \text{FSR}^{-1}$ is the roundtrip time, and $\alpha = (\alpha_i L + \theta)/2$ describes the total linear cavity losses with α_i the internal absorption, θ the coupler power transmission coefficient, and L the resonator roundtrip length. Defining ϕ_0 as the linear phase-shift acquired by light at the driving frequency over one roundtrip, $\delta_0 = 2\pi l - \phi_0$ measures the phase detuning of the driving field with respect to the closest linear resonance (with order l). The β_k 's are the Taylor series expansion coefficients of the resonator propagation constant about the angular frequency ω_0 of the driving field and γ is the non-linearity coefficient. Self-steepening was verified not to play a significant role with our parameters, and can be neglected.

To analyze comb stability we integrate Eq. (1) using the split-step Fourier method. For the sake of discussion, we consider a silicon nitride resonator with simulation parameters approximated from [5] and already used in [15]: loaded quality factor $Q = 3 \cdot 10^5$; $\text{FSR} = 226$ GHz; $\gamma = 1 \text{ W}^{-1} \text{ m}^{-1}$; $\alpha = \theta = 0.009$. The driving power is set to $P_{\text{in}} = |E_{\text{in}}|^2 = 755$ mW. We emphasize that the choice of parameters is immaterial: the LLE can be normalized as in [12, 16], extending our analysis to arbitrary configurations. Accordingly, we refer below to the normalized detuning $\Delta = \delta_0/\alpha$ and, as the relevant dynamical timescale, to the photon lifetime $t_{\text{ph}} = Q/\omega_0 = t_R/(2\alpha)$. Here $t_{\text{ph}} \simeq 56 t_R$. We have numerically explored the stability characteristics of all four classes of comb solutions of the LLE [16]. For increasing values of Δ , these are: (i) stable modulation instability (SMI); (ii) unstable modulation instability (UMI); (iii) unstable cavity solitons (UCS); and (iv) stable cavity solitons (SCS). For each detuning Δ , the simulation initial condition consists of the cw steady-state solution [the upper state when bistable, $\Delta > \sqrt{3}$] superimposed with

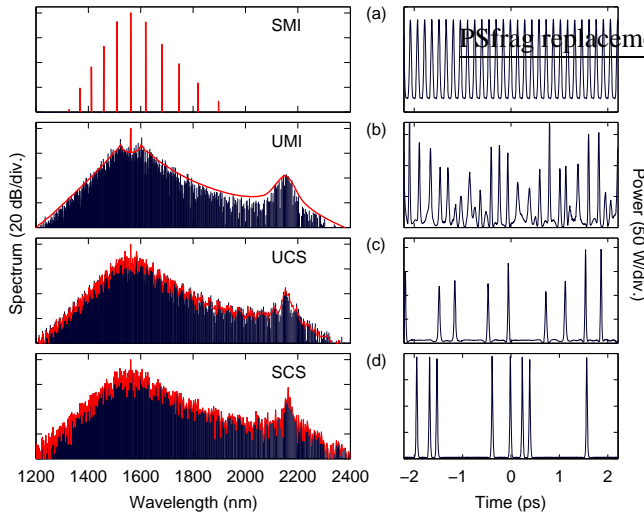


Fig. 1. Illustrative simulation results for $\Delta = -0.5, 3, 4,$ and 6 [from (a) to (d)]. Left: single roundtrip snapshot (black) and 1-million roundtrip averaged (red) spectra. Right: single-roundtrip snapshot of the corresponding temporal intensity profile.

a quantum noise seed of one photon with random phase per mode. To avoid transients, we simulate the intracavity dynamics over one million roundtrips (more than $17,000 t_{\text{ph}}$) before gathering stability statistics. We have verified this approach to yield qualitatively identical results as the more realistic (but more computationally intensive) method of ramping Δ to bring the driving laser into resonance [18, 19]. Note that we do not put noise on the driving field: the comb coherence we quantify here represents the intrinsic nonlinear cavity dynamics. Technical noise on the pump will further degrade the coherence. A detailed study will be presented elsewhere, but we have found this degradation to be relatively minor even with noise levels well above shot-noise.

Figure 1 shows simulated spectral and temporal characteristics illustrative of each regime of LLE solutions. The left panels show a spectral snapshot corresponding to a single roundtrip (black) as well as the *mean* spectrum averaged over 1 million roundtrips (red); the right panels show a snapshot of the time-domain intracavity field. Figure 1(a) corresponds to stable MI, obtained with $\Delta = -0.5$. The spectrum is dominated by “primary” comb lines separated by multiple FSRs [26]. The time-domain profile is a periodic pattern that repeats every roundtrip: the comb is stable. Correspondingly, the mean spectrum is identical to that of a single roundtrip. For an increased cavity detuning the MI solution becomes unstable [16]. Typical simulation results are shown in Fig. 1(b) for $\Delta = 3$. The mean spectrum is smooth, and contains a broad dispersive wave (DW) pedestal at 2140 nm [15]. We note that the mean spectrum closely resembles the experimental measurement in [5]. The comb is however unstable, and the smoothness of the spectrum arises from ensemble averaging of fluctuating, highly-structured single-roundtrip spectra [27]. Rapid fluctuations are also apparent in the time-domain snapshot. Above the upswitching point, $\Delta_{\uparrow} \simeq 3.2$ in our case, the nature of LLE solutions changes from MI to CSs [16]. Figure 1(c) shows results for $\Delta = 4$ in the unstable CS regime,

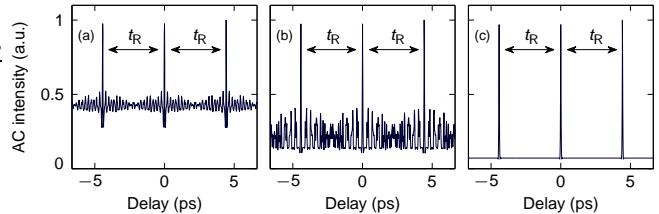


Fig. 2. Simulated AC traces for the (a) unstable MI, (b) unstable CS, and (c) stable CS regimes. The cavity detuning values correspond to those in Figs. 1(b)–(d).

characterized by breathing CSs [16, 28, 29] as alluded to by the time-domain snapshot. Here the breathing period is $3t_{\text{ph}}$ (or $167t_{\text{R}}$) for all CSs, though in general they oscillate out-of-sync. The mean spectrum is no longer smooth but exhibits sharp features. Finally, further increasing the detuning allows for the excitation of stable CSs [16–19]. Typical characteristics are shown in Fig. 1(d) for $\Delta = 6$. The mean spectrum is identical with an arbitrarily selected snapshot, and both exhibit complex structure owing to the multiple CSs populating the cavity. Naturally for a single CS the spectrum is smooth [15]. We find that the number of solitons generally varies with the input noise-seed, yet their characteristics remain the same. They all drift with the same small constant velocity in the τ -reference frame due to high-order dispersion [30]. Also, they do not experience *relative* motion, which ensures the stability of the comb. Extra sources of noise may however affect this.

Little insights can be obtained on comb stability based on the mean spectrum. The same applies to ensemble-averaged temporal measurements, as already mentioned in [19]. To highlight this point, we plot in Figs. 2(a)–(b) the averaged intensity autocorrelation (AC) traces corresponding to the unstable MI and CS regimes of Figs. 1(b)–(c), respectively. The AC traces are displayed over a temporal span of three roundtrips, and were computed from 5000 consecutive roundtrips. For comparison we also plot, in Fig. 2(c), the AC trace of a stable comb in which a single CS populates the cavity ($\Delta = 6$). In all cases the trace consists of sharp peaks atop a background, repeating at delays separated by the cavity roundtrip time (note that the background in the CS regime would be smaller for larger Q s). For the unstable regimes the peaks correspond to “coherence artefacts” and should not be confused with stable pulse formation [20]. They are periodic owing to the long photon-lifetime (high-finesse) of the cavity: the field changes slowly from roundtrip-to-roundtrip such that for delays of a few roundtrips the AC signal is almost identical to that at zero delay. Similar artefacts appear for time-averaged frequency-resolved optical gating measurements.

To examine the coherence of the simulated Kerr combs, we calculate the modulus of the complex degree of first-order coherence at each wavelength λ ,

$$|g_{12}^{(1)}(\lambda, t_1 - t_2)| = \frac{|\langle \tilde{E}^*(t_1, \lambda) \tilde{E}(t_2, \lambda) \rangle|}{S(\lambda)}. \quad (2)$$

Here, \tilde{E} is the complex Fourier transform of the intracavity (or output) electric field (both give the same result), the angle brackets denote an ensemble average, and $S(\lambda) = \langle |\tilde{E}(\lambda)|^2 \rangle$

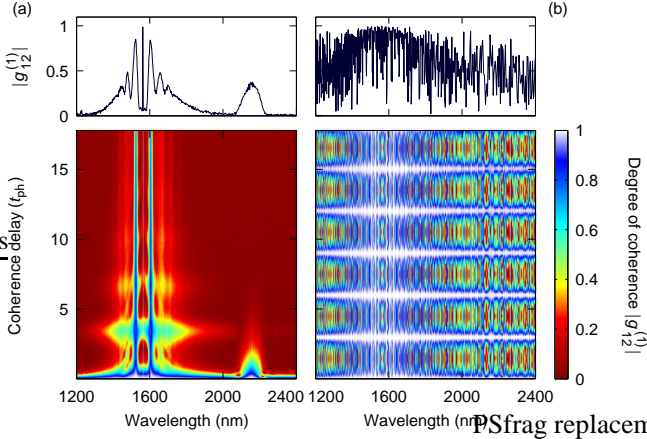


Fig. 3. Degree of first-order coherence across simulated Kerr combs as a function of coherence delay (density maps) and for a two photon-lifetime delay (line plot at the top) for (a) the unstable MI and (b) the unstable CS regimes. The corresponding mean spectra are shown in Fig. 1(b) and Fig. 1(c), respectively.

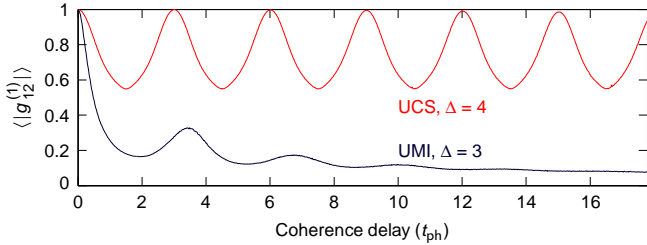


Fig. 4. Overall degree of coherence as a function of coherence delay for the unstable MI (black) and unstable CS (red) regimes.

is the mean spectrum. We evaluate $|g_{12}^{(1)}|$ at coherence delays $|t_1 - t_2| = nt_R$, where n is a positive integer (intermediate delays only affect the periodicity of the fringe pattern, not the visibility). In other words, we examine correlations between intracavity fields separated by a set number of cavity roundtrips. Note that this differs from SC coherence calculations in which all pairs of outputs are considered as the noise varies randomly from shot to shot [22], while for Kerr combs the sequence is deterministic and set by the cavity dynamics. The stable MI and CS regimes have almost perfect coherence, i.e., $|g_{12}^{(1)}(\lambda, nt_R)| = 1$ for all n, λ . To the contrary, the unstable regimes exhibit a complex dependence on both λ and n as illustrated in Fig. 3 for the same detunings as in Figs. 1(b)–(c). The density maps show $|g_{12}^{(1)}(\lambda, nt_R)|$ as a function of wavelength and coherence delay, while the line plots at the top show the degree of coherence for a selected delay corresponding to two photon lifetimes ($112t_R$). As expected based on the high cavity finesse, both regimes display strong correlations over small delays ($nt_R \ll t_{ph}$), in agreement with the presence of coherence artifacts in the AC traces of Figs. 2(a)–(b). The coherence of the unstable MI comb [Fig. 3(a)] rapidly degrades for larger delays. At $|t_1 - t_2| = 112t_R \sim 2t_{ph}$ the overall coherence is almost vanished with $|g_{12}^{(1)}| \sim 0$ over most of the comb. Residual coherence manifests only at the DW edge and for the first few primary comb lines, i.e., those experiencing maximum parametric gain. For even larger delays the

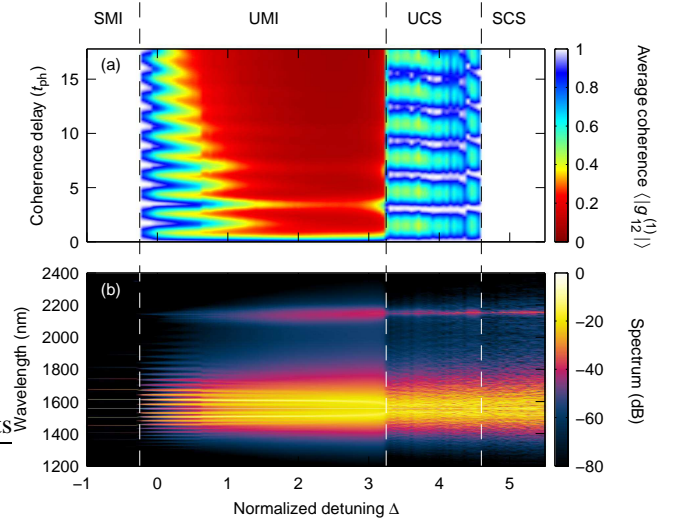


Fig. 5. (a) Overall degree of coherence over a wide range of cavity detunings. The corresponding mean spectra are shown in (b).

DW also becomes decorrelated, but the fundamental parametric sidebands remain quasi-coherent. The lack of fluctuations in the vicinity of these frequencies is also corroborated by the two sharp features in the mean spectrum plotted in Fig. 1(b).

An entirely different behavior is observed in the unstable (breathing) CS regime [Fig. 3(b)]. The degree of coherence degrades much more slowly than in the UMI regime and is periodically restored for increasing delays, here with a period of $3t_{ph}$. This period is found to match with the breathing period of the associated oscillatory CSs described above. Because the entire intracavity field repeats over the breathing period, strong correlations, $|g_{12}^{(1)}| \sim 1$, are expected at delays multiple of that period. The different coherence properties of the two regimes are further highlighted in Fig. 4 by considering the *overall coherence* $\langle |g_{12}^{(1)}(nt_R)| \rangle$ averaged over the exploitable comb. Specifically, we average $|g_{12}^{(1)}(\lambda, nt_R)|$ over wavelengths at which the mean comb power exceeds -80 dB (relative to the driving mode, see Fig. 1). The coherence oscillations of the unstable CS regime are clearly visible on the plot (red) while the overall coherence drops rapidly for the unstable MI regime (black), with a subsequent slow decline towards a quasi-incoherent value of $\langle |g_{12}^{(1)}(nt_R)| \rangle \sim 0.1$. Note that even this latter regime exhibits decaying coherence oscillations (with a period $3.5t_{ph}$) which are reminiscent of a breathing (Hopf) instability.

In order to show that the coherence properties described above are not specific to our examples but rather are characteristics of each representative comb regimes, we have repeated our analysis over a wide range of cavity detunings. Our results are summarized in Fig. 5. Specifically, in Fig. 5(a) we show the overall degree of coherence as a function of coherence delay and cavity detuning, while Fig. 5(b) displays the corresponding mean spectrum. The four distinct classes of LLE solutions can be clearly evidenced from both graphs, as highlighted. The coherence in the UMI regime deteriorates progressively for increased cavity detuning, before being abruptly ameliorated on transition to the UCS

regime, at a detuning corresponding to the cw upswitching point ($\Delta_{\uparrow} \simeq 3.2$). In contrast, the level of coherence changes smoothly between stable and unstable solutions of the same family (MI or CSs). Islands of varying coherence visible in the UCS regime are due to the stochastic nature of our simulations: different configurations of CSs are excited depending on the initial noise-seed as well as the detuning Δ . In particular, a range of multiple-CS bound states emerge in varying numbers. Local variations in the overall comb coherence follow because bound CSs appear to exhibit degraded coherence compared to isolated CSs. This observation may be explained by differences in the Hopf threshold of bound and isolated CS states, with the former typically occurring at a higher detuning and defining the upper boundary of the UCS regime.

Our results have a number of important implications. On the one hand, it is clear that Kerr combs in the unstable MI or CS regimes are undesirable owing to the spectral and temporal fluctuations intrinsic to both. On the other hand, our results show that the unstable CS regime exhibits coherence which is greatly improved from that of MI. This observation raises a critical warning, because past studies have associated a drop in the low-frequency radio frequency spectrum as evidence of stable pulse formation. In light of our results, such observations could correspond to the transition from unstable MI to *unstable* CSs. The difficulty of unambiguously evidencing a stable soliton state is further compounded by potential pitfalls in ensemble-averaged time-domain measurements. The use of the complex degree of first-order coherence, as proposed here, alleviates all these deficiencies, and offers a rapid route towards broadband comb characterization. We emphasize that $|g_{12}^{(1)}(\lambda)|$ is readily accessible experimentally from the visibility of spectral interference fringes, requiring only a standard optical spectrum analyzer and a delayed interferometer [24, 25]. From our results, a temporal delay of the order of a few photon lifetimes is sufficient to discern between the different regimes. Q is the dominant factor in $t_{\text{ph}} = Q/\omega_0$. The largest delays are thus required for crystalline resonators, which exhibit the highest Q -factors. Taking $Q = 10^9$ yields $t_{\text{ph}} = 0.82 \mu\text{s}$ (at 1550 nm). Such delays can be routinely obtained using a fiber-based interferometer [31]. Lower- Q resonators, like the silicon nitride device considered in our analysis above, require much shorter delays of a few tenth of nanoseconds, readily accessible in bulk. We therefore expect experimental measurements of Kerr comb coherence soon to follow. Finally, we note that additional insights on the mutual coherence of distinct comb frequencies may also be obtained via the use of two-dimensional correlation functions of second-order coherence theory [32, 33]. This will be explored in a future work.

We acknowledge support from the Marsden Fund of the Royal Society of New Zealand.

References

1. T. J. Kippenberg, R. Holzwarth, and S. A. Diddams, *Science* **332**, 555–559 (2011).
2. P. Del’Haye, A. Schliesser, O. Arcizet, T. Wilken, R. Holzwarth, and T. J. Kippenberg, *Nature* **450**, 1214–1217 (2007).
3. A. A. Savchenkov, A. B. Matsko, V. S. Ilchenko, I. Solomatine, D. Seidel, and L. Maleki, *Phys. Rev. Lett.* **101**, 093902 (2008).
4. P. Del’Haye, T. Herr, E. Gavartin, M. L. Gorodetsky, R. Holzwarth, and T. J. Kippenberg, *Phys. Rev. Lett.* **107**, 063901 (2011).
5. Y. Okawachi, K. Saha, J. S. Levy, Y. H. Wen, M. Lipson, and A. L. Gaeta, *Opt. Lett.* **36**, 3398–3400 (2011).
6. F. Ferdous, H. Miao, D. E. Leaird, K. Srinivasan, J. Wang, L. Chen, L. T. Varghese, and A. M. Weiner, *Nat. Photon.* **5**, 770–776 (2011).
7. S. B. Papp and S. A. Diddams *Phys. Rev. A* **84**, 053833 (2011).
8. T. Herr, K. Hartinger, J. Riemensberger, C. Y. Wang, E. Gavartin, R. Holzwarth, M. L. Gorodetsky, and T. J. Kippenberg, *Nat. Photon.* **6**, 480–487 (2012).
9. I. S. Grudinin, L. Baumgartel, and N. Yu, *Opt. Express* **20**, 6604–6609 (2012).
10. K. Saha, Y. Okawachi, B. Shim, J. S. Levy, R. Salem, A. R. Johnson, M. A. Foster, M. R. E. Lamont, M. Lipson, and A. L. Gaeta, *Opt. Express* **21**, 1335–1343 (2013).
11. S. Wabnitz, *Opt. Lett.* **18**, 601–603 (1993).
12. F. Leo, S. Coen, P. Kockaert, S.-P. Gorza, Ph. Emplit, and M. Haelterman, *Nat. Photon.* **4**, 471–476 (2010).
13. J. K. Jang, M. Erkintalo, S. G. Murdoch, and S. Coen, *Nat. Photon.* **7**, 657–663 (2013).
14. A. B. Matsko, A. A. Savchenkov, W. Liang, V. S. Ilchenko, D. Seidel, and L. Maleki, *Opt. Lett.* **36**, 2845–2847 (2011).
15. S. Coen, H. G. Randle, T. Sylvestre, and M. Erkintalo, *Opt. Lett.* **38**, 37–39 (2013).
16. S. Coen and M. Erkintalo, *Opt. Lett.* **38**, 1790–1792 (2013).
17. Y. K. Chembo and C. R. Menyuk, *Phys. Rev. A* **87**, 053852 (2013).
18. M. R. E. Lamont, Y. Okawachi, and A. L. Gaeta, *Opt. Lett.* **38**, 3478–3481 (2013).
19. T. Herr, V. Brasch, J. D. Jost, C. Y. Wang, N. M. Kondratiev, M. L. Gorodetsky, and T. J. Kippenberg, arXiv: 1211.0733.
20. M. Rhodes, G. Steinmeyer, J. Ratner, and R. Trebino, *Laser and Photon. Rev.* **7**, 557565 (2013).
21. M. Bellini and Th. W. Hänsch, *Opt. Lett.* **25**, 1049–1051 (2000).
22. J. M. Dudley and S. Coen, *Opt. Lett.* **27**, 1180–1182 (2002).
23. J. M. Dudley, G. Genty, and S. Coen, *Rev. Mod. Phys.* **78**, 1135–1184 (2006).
24. X. Gu, M. Kimmel, A. P. Shreenath, R. Trebino, J. M. Dudley, S. Coen, and R. S. Windeler, *Opt. Express* **11**, 2697–2703 (2003).
25. F. Lu and W. H. Knox, *Opt. Express* **12**, 347–353 (2004).
26. Y. K. Chembo and N. Yu, *Phys. Rev. A* **82**, 033801 (2010).
27. A. B. Matsko, W. Liang, A. A. Savchenkov, and L. Maleki, *Opt. Lett.* **38**, 525–527 (2013).
28. A. B. Matsko, A. A. Savchenkov, and L. Maleki, *Opt. Lett.* **37**, 4856–4858 (2012).
29. F. Leo, L. Gelens, Ph. Emplit, M. Haelterman, and S. Coen, *Opt. Express* **21**, 9180 (2013).
30. F. Leo, A. Mussot, P. Kockaert, Ph. Emplit, M. Haelterman, and M. Taki, *Phys. Rev. Lett.* **110**, 104103 (2013).
31. A. F. J. Runge, C. Aguergeray, N. G. R. Broderick, and M. Erkintalo, *Opt. Lett.* **38**, 4327–4330 (2013).
32. G. Genty, M. Surakka, J. Turunen, and A. T. Friberg, *J. Opt. Soc. Am. B* **28**, 2301–2309 (2011).
33. M. Erkintalo, M. Surakka, J. Turunen, A. T. Friberg, and G. Genty *Opt. Lett.* **37**, 169–171 (2012).

References

1. T. J. Kippenberg, R. Holzwarth, and S. A. Diddams, "Microresonator-based optical frequency combs," *Science* **332**, 555–559 (2011).
2. P. Del'Haye, A. Schliesser, O. Arcizet, T. Wilken, R. Holzwarth, and T. J. Kippenberg, "Optical frequency comb generation from a monolithic microresonator," *Nature* **450**, 1214–1217 (2007).
3. A. A. Savchenkov, A. B. Matsko, V. S. Ilchenko, I. Solomatine, D. Seidel, and L. Maleki, "Tunable optical frequency comb with a crystalline whispering gallery mode resonator," *Phys. Rev. Lett.* **101**, 093902 (2008).
4. P. Del'Haye, T. Herr, E. Gavartin, M. L. Gorodetsky, R. Holzwarth, and T. J. Kippenberg, "Octave spanning tunable frequency comb from a microresonator," *Phys. Rev. Lett.* **107**, 063901 (2011).
5. Y. Okawachi, K. Saha, J. S. Levy, Y. H. Wen, M. Lipson, and A. L. Gaeta, "Octave-spanning frequency comb generation in a silicon nitride chip," *Opt. Lett.* **36**, 3398–3400 (2011).
6. F. Ferdous, H. Miao, D. E. Leaird, K. Srinivasan, J. Wang, L. Chen, L. T. Varghese, and A. M. Weiner, "Spectral line-by-line pulse shaping of on-chip microresonator frequency combs," *Nat. Photon.* **5**, 770–776 (2011).
7. S. B. Papp and S. A. Diddams "Spectral and temporal characterization of a fused-quartz-microresonator optical frequency comb," *Phys. Rev. A* **84**, 053833 (2011).
8. T. Herr, K. Hartinger, J. Riemensberger, C. Y. Wang, E. Gavartin, R. Holzwarth, M. L. Gorodetsky, and T. J. Kippenberg, "Universal formation dynamics and noise of Kerr-frequency combs in microresonators," *Nat. Photon.* **6**, 480–487 (2012).
9. I. S. Grudin, L. Baumgartel, and N. Yu, "Frequency comb from a microresonator with engineered spectrum," *Opt. Express* **20**, 6604–6609 (2012).
10. K. Saha, Y. Okawachi, B. Shim, J. S. Levy, R. Salem, A. R. Johnson, M. A. Foster, M. R. E. Lamont, M. Lipson, and A. L. Gaeta, "Modelocking and femtosecond pulse generation in chip-based frequency combs," *Opt. Express* **21**, 1335–1343 (2013).
11. S. Wabnitz, "Suppression of interactions in a phase-locked soliton optical memory," *Opt. Lett.* **18**, 601–603 (1993).
12. F. Leo, S. Coen, P. Kockaert, S.-P. Gorza, Ph. Emplit, and M. Haelterman, "Temporal cavity solitons in one-dimensional Kerr media as bits in an all-optical buffer," *Nat. Photon.* **4**, 471–476 (2010).
13. J. K. Jang, M. Erkintalo, S. G. Murdoch, and S. Coen, "Ultra-weak long-range interactions of solitons observed over astronomical distances," *Nat. Photon.* **7**, 657–663 (2013).
14. A. B. Matsko, A. A. Savchenkov, W. Liang, V. S. Ilchenko, D. Seidel, and L. Maleki, "Mode-locked Kerr frequency combs," *Opt. Lett.* **36**, 2845–2847 (2011).
15. S. Coen, H. G. Randle, T. Sylvestre, and M. Erkintalo, "Modeling of octave-spanning Kerr frequency combs using a generalized mean-field Lugiato-Lefever model," *Opt. Lett.* **38**, 37–39 (2013).
16. S. Coen and M. Erkintalo, "Universal scaling laws of Kerr frequency combs," *Opt. Lett.* **38**, 1790–1792 (2013).
17. Y. K. Chembo and C. R. Menyuk, "Spatiotemporal Lugiato-Lefever formalism for Kerr-comb generation in whispering-gallery-mode resonators," *Phys. Rev. A* **87**, 053852 (2013).
18. M. R. E. Lamont, Y. Okawachi, and A. L. Gaeta, "Route to stabilized ultrabroadband microresonator-based frequency combs," *Opt. Lett.* **38**, 3478–3481 (2013).
19. T. Herr, V. Brasch, J. D. Jost, C. Y. Wang, N. M. Konradiev, M. L. Gorodetsky, and T. J. Kippenberg, "Mode-locking in an optical microresonator via soliton formation," arXiv: 1211.0733.
20. M. Rhodes, G. Steinmeyer, J. Ratner, and R. Trebino, "Pulse-shape instabilities and their measurement," *Laser and Photon. Rev.* **7**, 557565 (2013).
21. M. Bellini and Th. W. Hänsch, "Phase-locked white-light continuum pulses: toward a universal optical frequency-comb synthesizer," *Opt. Lett.* **25**, 1049–1051 (2000).
22. J. M. Dudley and S. Coen, "Coherence properties of supercontinuum spectra generated in photonic crystal and tapered optical fibers," *Opt. Lett.* **27**, 1180–1182 (2002).
23. J. M. Dudley, G. Genty, and S. Coen, "Supercontinuum generation in photonic crystal fiber," *Rev. Mod. Phys.* **78**, 1135–1184 (2006).
24. X. Gu, M. Kimmel, A. P. Shreenath, R. Trebino, J. M. Dudley, S. Coen, and R. S. Windeler, "Experimental studies of the coherence of microstructure-fiber supercontinuum," *Opt. Express* **11**, 2697–2703 (2003).
25. F. Lu and W. H. Knox, "Generation of a broadband continuum with high spectral coherence in tapered single-mode optical fibers," *Opt. Express* **12**, 347–353 (2004).
26. Y. K. Chembo and N. Yu, "Modal expansion approach to optical-frequency-comb generation with monolithic whispering-gallery-mode resonators," *Phys. Rev. A* **82**, 033801 (2010).
27. A. B. Matsko, W. Liang, A. A. Savchenkov, and L. Maleki, "Chaotic dynamics of frequency combs generated with continuously pumped nonlinear microresonators," *Opt. Lett.* **38**, 525–527 (2013).
28. A. B. Matsko, A. A. Savchenkov, and L. Maleki, "On excitation of breather solitons in an optical microresonator," *Opt. Lett.* **37**, 4856–4858 (2012).
29. F. Leo, L. Gelens, Ph. Emplit, M. Haelterman, and S. Coen, "Dynamics of one-dimensional Kerr cavity solitons," *Opt. Express* **21**, 9180 (2013).
30. F. Leo, A. Mussot, P. Kockaert, Ph. Emplit, M. Haelterman, and M. Taki, "Nonlinear symmetry breaking induced by third-order dispersion in optical fiber cavities," *Phys. Rev. Lett.* **110**, 104103 (2013).
31. A. F. J. Runge, C. Agueraray, N. G. R. Broderick, and M. Erkintalo, "Coherence and shot-to-shot spectral fluctuations in noise-like ultrafast fiber lasers," *Opt. Lett.* **38**, 4327–4330 (2013).
32. G. Genty, M. Surakka, J. Turunen, and A. T. Friberg, "Complete characterization of supercontinuum coherence," *J. Opt. Soc. Am. B* **28**, 2301–2309 (2011).
33. M. Erkintalo, M. Surakka, J. Turunen, A. T. Friberg, and G. Genty "Coherent-mode representation of supercontinuum," *Opt. Lett.* **37**, 169–171 (2012).